Japan-Philippine Joint Workshop on Materials for Safe and Sustainable Society 2011

Shizuoka University, Hamamatsu, Japan
December 5, 2011

Supported by Japan Student Service Organization
and Shizuoka University

Proceedings of Japan-Philippine Joint Workshop on Materials for Safe and Sustainable Society 2011

December 5, 2011

Shizuoka University, Hamamatsu, Shizuoka, Japan

Organized by
Division of Mechanics and Strength of Materials, Department of Mechanical Engineering, Shizuoka University

Sponsored by
Japan Student Service Organization, Japan
Shizuoka University, Japan

Outline of the Workshop

10:30-10:40 Opening Address (Prof. Tohgo)
10:40-11:55 Oral Presentation Session I
11:55-13:00 Lunch
13:00-14:15 Oral Presentation Session II
14:15-14:30 Coffee Break
14:30-15:30 Oral Presentation Session III
15:30-15:40 Closing Address (Prof. Shimamura)
19:00-21:00 Banquet (Dinning Pub Irohanihoheto)

Program

Oral Presentation Session I (Chair Prof. Shimamura, Shizuoka University)

10:40-10:55

M.Kim, T.Fujii, K.Tohgo and Y.Shimamura
(Shizuoka University)
"*Applicability of Non-linear Fracture Mechanics in Stress Corrosion Cracking Behavior of Austenitic Stainless Steel*" ····· 1

10:55-11:10

J.K.C.N.Agutaya and T.P.Tumolva
(University of the Philippines-Diliman)
"*Non-isothermal Kinetic Parameters of Unsaturated Polyester Using Modified Coats-Redfern Method*" ····· 3

11:10-11:25

A.Kokobo, Y.Shimamura, S.Kamada, H.Masuda, H.Ishii, K.Tohgo, T.Fujii, T.Yagasaki and M.Harada
(Shizuoka University)
"*Development of Ultrasonic Torsion Fatigue Testing Machine*" ····· 5

Applicability of Non-linear Fracture Mechanics in Stress Corrosion Cracking Behavior of Austenitic Stainless Steel

Minjung KIM[*1], Tomoyuki FUFII[*1], Keiichiro TOHGO[*1] and Yoshinobu SHIMAMURA[*1]

[*1]Shizuoka University Department of Mechanical Engineering
3-5-1 Johoku Naka-ku, Hamamatsu, 432-8561.Japan
e-mail: kim@mechmat.eng.shizuoka.ac.jp

1. Introduction

Growth behavior of stress corrosion cracking (SCC) is commonly evaluated by stress intensity factor. However, SCC initiates and propagates in plastic deformation field. The effect of plastic deformation on the SCC growth behavior is not clear.

This paper deals with the evaluation of SCC growth rate taking account of plastic deformation field. Two kinds of SCC growth test in corrosion liquid were conducted and SCC growth rate was arranged by stress intensity factor and equivalent stress intensity factor, which was calculated from J integral. The effect of plastic deformation on SCC growth rate was evaluated by comparison between stress intensity factor and equivalent stress intensity factor.

2. Experimental procedure

2.1 Material

Stainless-steel type 304 was used for SCC growth test. solution heat treatment of 1100℃ for 45 minutes and sensitization treatment of 600℃ for 16 hours were conducted.

2-2 Test environment

SCC growth test was conducted in corrosive liquid which was 1% polythionic acid and adjusted to pH=3. The liquid exchanged for new liquid every 48 hours.

2-3 Wedge opening loading test

Figure 1 shows the WOL (Wedge opening load) specimen. The load corresponds to the stress intensity factor of 22, 30 and 40 $MPam^{0.5}$ was applied, and the specimen was immersed in the corrosive liquid. The crack length was measured every 1 hour.

2-4 Four-point bending test

Figure 2 shows the four point bending specimen. The specimen with shallow notch, which is 0.5 mm deep, was used to investigate the single crack growth from the notch root. Strain of 1% at the compressive surface was applied and the specimen was also immersed in the corrosive liquid. The crack length from the notch root was measured every 1 hour.

3. Results and Discussion

Figure 3 shows SCC growth rate a function of stress intensity factor. The stress intensity factor of the WOL tests[(1)] and four-point bending tests[(2)] was calculated by load and crack length. The SCC growth rate of the WOL tests increased with increasing stress intensity factor. On the other

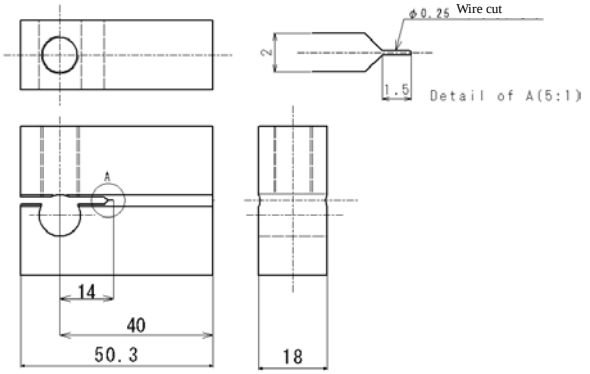

Fig. 1 WOL specimen.

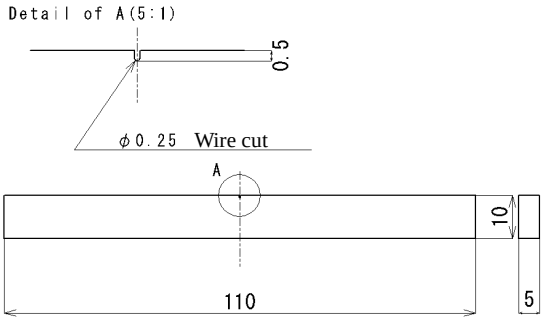

Fig. 2 Four-point-bending specimen

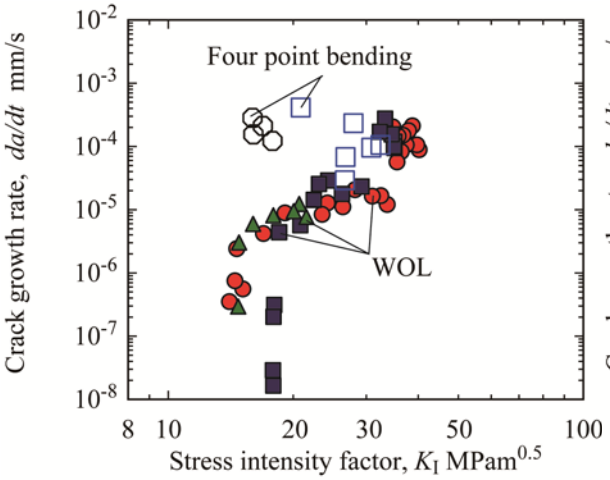

Fig. 3 *da/dt – K*

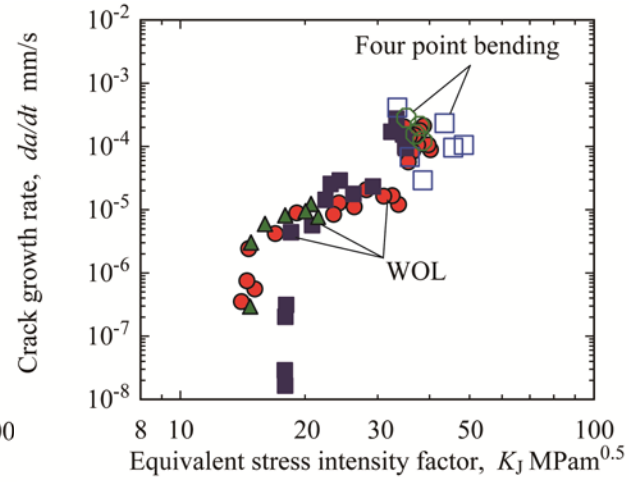

Fig. 4 *da/dt - K_J*

hand, the crack growth rate of the four point bending tests was almost constant irrespective stress intensity factor. The crack growth rate of the four point bending tests was about ten times faster than that of the WOL tests for the same stress intensity factor. It is considered that the effect of plastic deformation is neglected.

Figure 4 shows SCC growth rate a function of equivalent stress intensity factor. The equivalent stress intensity factor was calculated as follows;

$$K_J = \sqrt{EJ} \quad (1)$$

where E and J are the Young's modulus and J integral, respectively. The value of J integral was calculated by finite element analysis. In the WOL tests, the equivalent stress intensity factor is equal to the stress intensity factor because of the small scale yielding condition. The plots of SCC growth rate of four point bending tests shift rightward and the results of the point bending tests agrees with those of the WOL tests. Because the equivalent stress intensity factor is the parameter taking account of plastic deformation. Therefore, the plastic deformation affects the SCC growth rate, and it is valid to evaluate the SCC behavior based on J integral or effective stress intensity factor.

Reference

1. P. W. Holsberg, R. A. Hays, Development of Compliance Expression for Deeply Flawed 1T-WOL Specimen, NAVAL SURFACE WARFARE CENTER CARDEROCK DIV BETHESDA, CAE-DIVNSWC-TR-61-1999-20
2. H. Tada, P. C. Rice and G. Irwin, The stress analysis of cracks handbook, Del Research, pp.2-14, (1985).

Non-isothermal Kinetic Parameters of Unsaturated Polyester Using Modified Coats-Redfern Method

Jonas Karl Christopher N. Agutaya* and Terence P. Tumolva

Department of Chemical Engineering, University of the Philippines
Diliman 1101 Quezon City, Philippines
TELEFAX: +63-2-929-6640
e-mail: jnagutaya@gmail.com

1. Introduction

Polyesters and epoxies are petrochemicals that account for 95% of the thermoset composite market with the former predominating in volume by about ten-fold. The production of these synthetic thermosets is largely dependent on the status of the oil industry. With the current trend of increasing oil price, their production cost is bound to rise as well. Furthermore, global environmental concerns, particularly non-biodegradable landfill impact, have come up regarding thermosets. These problems of limited resource and disposal can be addressed by improving the efficiency of the process and recycling or by thermal decomposition, respectively. These solutions require knowledge on the mechanism function and, by extension, the kinetic parameters of the material.

This study focuses on the application of an improved iterative version of the Coats-Redfern method to compute for the non-isothermal kinetic parameters for orthophthalic unsaturated polyester (ortho-UP) based on TGA data.

2. Derivation of Objective Function

The dependence of the degree of conversion α on the temperature *T* and the heating rate β can be described by the following differential equation:

$$\frac{d\alpha}{dT} = \left(\frac{A}{\beta}\right) f(\alpha) \exp\left(-\frac{E}{RT}\right) \quad (1)$$

where *A* is the pre-exponential factor, *E* is the activation energy, and *f*(α) is the differential conversion function, which characterizes the reaction mechanism.

By variable separation and integration, Eq. (1) becomes

$$g(\alpha) \equiv \int_0^{\alpha} \frac{d\alpha}{f(\alpha)} = \left(\frac{A}{\beta}\right) \int_0^{T_0} \exp\left(-\frac{E}{RT}\right) dT \quad (2)$$

where $g(\alpha)$ is the integral conversion function.

The integral on the left-hand side of Eq. (2) has no exact analytical solution, but can be approximated as follows:

$$\left(\frac{A}{\beta}\right) \int_0^{T_0} \exp\left(-\frac{E}{RT}\right) dT = \frac{AE}{R\beta} \frac{\exp(-x)}{x} Q(x) \quad (3)$$

$$Q(x) = \frac{x^4 + 18x^3 + 86x^2 + 86x}{x^4 + 20x^3 + 120x^2 + 240x + 120} \quad (4)$$

Eqn. (3) and (4) are the fourth Senum and Yang approximation as presented in [1].

Substituting Eq. (3) into Eq. (2) gives

$$g(\alpha) = \left(\frac{AE}{R\beta}\right) \frac{\exp(-x)}{x^2} Q(x) \quad (5)$$

By taking the natural logarithm of both sides and rearranging some terms, Eq. (6) can be obtained.

$$\ln\left[\frac{g(\alpha)}{T^2}\right] - \ln\left[Q\left(\frac{E}{RT}\right)\right] - \ln\left(\frac{AR}{E\beta}\right) + \frac{E}{RT} = 0 \quad (6)$$

This will serve as the objective function in minimizing the sum of the squares of the residual terms, S_{res}, which is expressed in the following equation:

$$S_{res} = \sum_{i=1}^{N} \left\{ \ln\left[\frac{g(\alpha_i)}{T_i^2}\right] - \ln\left[Q\left(\frac{E}{RT_i}\right)\right] - a + \frac{b}{T_i} \right\}^2 \quad (7)$$

3. Results and Discussions

The TGA data used in the simulation was taken from [3]. The S_{res} function was minimized to give obtain the values of *a* and *b* for different heating rates. From each of these parameters, the average values of *E* and *R* were calculated to be 55,045.24 J mol^{-1} and 3421.25 min^{-1}, respectively.

Fig. 1 shows the profile of the heating rate as function of the inverse of temperature. The plot shows a linear correspondence between the two variables.

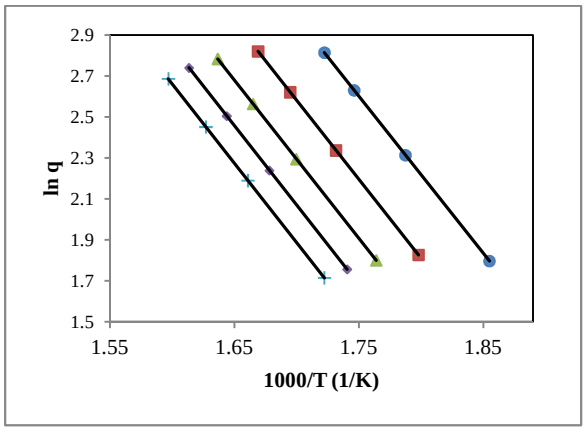

Fig. 1. Heating rate profile based on the computed kinetic parameters, *E* and *A*. Each line represents a constant degree of conversion. (●) – 30%, (■) – 25%, (▲) – 20%, (♦) – 15%, and (+) – 10%.

Superimposing the curves in Fig. 1 with a plot based on experimental data shows a significantly large deviation of the model. The values showed an average percent deviation of 1410% when compared point-by-point with the experimental data.

4. Conclusion

The iterative version of the Coats-Redfern method coupled with the fourth Yang and Senum approximations was not able to model the behaviour of the heating rate with changes in temperature. Thus, the procedure produced inaccurate values of the activation energy *R* and the Arrhenius constant *A*.

References

[1] E. Urbanovici, C. Popescu and E. Segal, J. of Therm. Anal. and Cal. **58** (1999) 683-700.

[2] S. Ch. Turmanova, S. D. Genieva, A. S. Dimitrova and L. T. Vlaev, eXPRESS Polymer Letters **2** (2008) 133-146.

[3] T. Tumolva, M. Kubouchi, S. Aoki, and T. Sakai (2011). "Evaluating the Carbon Storage Potential of Furan Resin-Based Green Composites". *18th International Conference on Composite Materials.*

Development of Ultrasonic Torsion Fatigue Testing Machine

Akito KOKUBO[1*], Yoshinobu SHIMAMURA[1], Shingo KAMADA[1], Hiroki MASUDA[1], Hitoshi ISHII[2] , Keiichiro TOHGO[1], Tomoyuki FUJII[1], Tooru YAGASAKI[3] and Masamichi HARADA[3]

[1] Department of Mechanical Engineering, Shizuoka University
3-5-1 Johoku, Naka-ku, Hamamatsu, Shizuoka 432-8561, Japan
[2]Professor Emeritus, Shizuoka University
[3]Honda R&D Co., Ltd
[*]e-mail: akokubo@mechmat.eng.shizuoka.ac.jp

1. Introduction

Recently, fatigue failure due to gigacycle (more than 10^7 cycles) loading have been reported. It is necessary to investigate gigacycle fatigue. However, the loading frequency of conventional fatigue testing machines is around 20Hz. It takes 19 months to achieve gigacycle. Therefore, developing a new method that can accelerate fatigue testing is required.

In this study, we have developed an ultrasonic torsional fatigue testing machine. The cyclic frequency of the testing machine is around 20 kHz. So it takes only 14 hours to achieve gigacycle and this machine enables us to accelerate fatigue testing considerably.

2. Ultrasonic Torsion Fatigue Testing Machine

Configuration of ultrasonic torsion fatigue testing machine is shown in Fig.1. The main components of the ultrasonic torsion fatigue testing machine are a signal generator, a torsional oscillator, an amplifying horn and a specimen. A signal generator generates electronic signal at the resonance frequency of the horn and specimen. Torsional oscillator converts the electronic signal into a torsional displacement at the same frequency. Thus cyclic loading can be applied to the specimen due to resonation. Since the torsional displacment generated by the oscillator is small, the torsional displacement is amplified by decreasing the sectional area of horn and specimen as shown in Fig.2.

Since generation of heat was remarkable during test, duty time and pause time were set to suppress temperature increase within the allowable range (i.e. less than 100°C in the case of steel). If the torsion amplitude felt below a threshold, the test stopped.

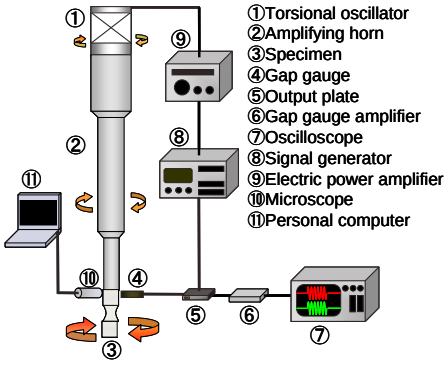

Fig. 1 Ultrasonic torsion fatigue testing machine.

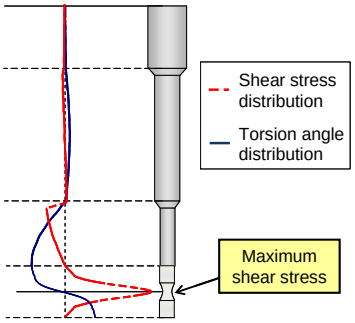

Fig. 2 Shear stress and torsion angle distribution.

3. New Testing Machine with Automatic Control

The existing ultrasonic torsion fatigue testing machine is controlled manually. Thus, the testing machine cannot follow the change of the resonance frequency caused by room temperature change. Besides, maximum shear stress applied by the testing machine is about 800MPa. Higher shear stress is required to investigate the higher strength steels.

To solve these problems, we are going to develop a new ultrasonic torsion testing machine. This testing machine adopts a signal generator that can automatically turn the resonance frequency and can follow the change of the resonance frequency. Moreover, the torsional oscillator has higher output and then be able to apply more than 1000MPa of shear stress to the specimen.

4. Application

With an ultrasonic torsion fatigue testing machine, the maximum shear stress arises on the surface of a specimen because of torsion. It is suitable to investigate the effect of surface treatment (i.e. carburizing or coating) on fatigue property.

Since the testing machine can apply higher shear stress than 800MPa, it enables us to conduct fatigue testing for higher strength steels during short period.

5. Conclusion

We are going to develop a new testing machine with automatic control.

Dip Coating of TiO_2 Photocatalyst on Glass Raschig Rings for Flow Photocatalytic Reactor Application

Patrick D. Ramoso and Maria Lourdes P. Dalida*

Department of Chemical Engineering, College of Engineering, University of the Philippines, Diliman, Quezon City 1101, Philippines
TEL&FAX: +63-2-929-6640
*e-mail: mpdalida@up.edu.ph

1. Introduction

With the decreasing supply of clean water due to pollution from industrial effluents, the challenge of developing an efficient wastewater treatment process has been widely studied in the past years. Photocatalysis has been extensively studied for its application to the removal of organic and inorganic contaminants from water [1]. Many organic pollutants in water can be completely decomposed at the surface of UV-irradiated TiO_2; these include alkanes, haloalkanes, aliphatic alcohols, carboxylic acids, alkenes, aromatics, haloaromatics, polymers, surfactants, herbicides, pesticides and dyes [2].

The heterogeneous photocatalytic reaction starts with the excitation of the TiO_2 catalyst by ultraviolet light with energies greater than or equal to the band gap energy ($E_{ph} \geq E_{bg}$), leading to the generation of mobile electrons (e^-) in the higher energy conduction band (E_{cb}) and positive holes (h^+) in the lower energy valence band (E_{vb}) [3].

$$photocatalyst \rightarrow e^- + h^+ \quad (1)$$

The formation of the electron-hole pairs leads to the generation of hydroxyl (·OH) radicals.

The adsorbed hydroxyl radicals are very reactive and oxidize the adsorbed substrates (RX_{ad}) into mineral acids including carbon dioxide and water:

$$\bullet OH_{ad} + RX_{ad} \rightarrow CO_2 + H_2O \quad (2)$$

The recombination of the electron and electron-hole is undesired and may lead to wasted energy and process inefficiency [3].

The photocatalyst could either be suspended in a slurry or immobilized on a support. Slurry systems require a post-process separation such as filtration to separate the catalyst. In an immobilized system, there is continuous operation and no need for an additional separation process, but it may be vulnerable to catalyst wash out [3].

The degradation of methylene blue in water by Degussa P25 TiO_2 in a batch slurry reactor has been observed and optimized in a previous study. The optimum parameters were found to be 20.6 mg/L initial MB concentration, pH 9.76 and catalyst loading of 6.82 g/L, which resulted to a decolorization efficiency of 97.6% [4].

In this study, Degussa P25 TiO_2 photocatalyst was immobilized on glass Raschig rings using various dip-coating media. The fabricated catalysts are subsequently analyzed using an FTIR spectrometer to characterize the catalyst.

2. Experimental

Degussa P25 TiO_2 (25% rutile, 75% anatase) were obtained as the photocatalyst to be coated on a glass Raschig rings approximately ¼ inch in diameter as support. Various dip coating media listed in Table 1 were used to immobilize the TiO_2.

Table 1. Dip coating media

A	TiO_2-water slurry (1 % wt.)
B	TiO_2-water mixture with cornstarch
C	TiO_2 mixture with silicone adhesive as binder and paint thinner as dilutant

The prepared catalyst was subjected to Fourier Transform Infrared (FTIR) spectroscopy using a Thermo Scientific Nicolet 6700 FT-IR spectrometer. Also subjected to FTIR analysis are samples of blank Raschig rings and Degussa P25 TiO_2.

3. Results and Discussion

The resulting catalysts were observed to be problematic in terms of the binding of the

coating medium with the Raschig rings. For catalyst A, the TiO_2 could be removed from the Raschig ring by hand. For catalyst B, the product showed lumps, as opposed to the desired film-like coating. In addition, the calcined coat B product contained black spots, indicating an incomplete degradation of cornstarch. For coat medium C, the TiO_2 coating cracked and flaked out.

As a reference, the FTIR spectra of the blank Raschig ring sample and the Degussa P25 TiO_2 sample are provided in Fig. 1. Figs. 2, 3, and 4 show the FTIR spectra of the product catalyst using coat medium A, B and C, respectively, with respect to the blank Raschig ring sample, and the difference of the spectra.

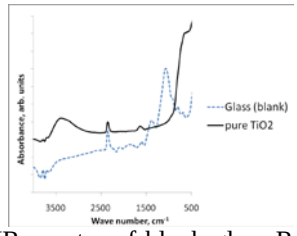

Fig. 1. FTIR spectra of blank glass Raschig ring and Degussa P25 TiO_2 samples

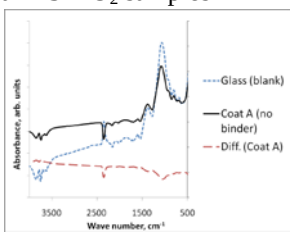

Fig. 2. FTIR spectra of calcined catalyst using Coat A , blank Raschig ring, and their difference

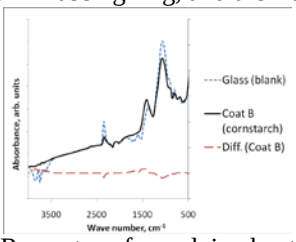

Fig. 3. FTIR spectra of uncalcined catalyst using Coat B, blank Raschig ring, and their difference

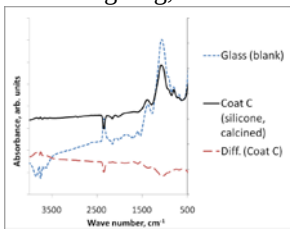

Fig. 4. Wide FTIR spectra of calcined catalyst using Coat C (silicone binder), blank glass Raschig ring, and their difference

Of particular interest in spectra above is the wave number at 2345 cm^{-1}, as the absorbance of the product A and C (Figs. 2 and 4) dropped, instead of an increase, as seen in the blank Raschig ring sample. In addition, the Degussa P25 TiO_2 sample also contained a peak on the same wave number. It is thus suggested that some reaction took place in catalyst fabrication that caused the material to have an opposing absorbance behavior at the given wave number.

In Fig. 3, the peak at 2345 cm^{-1} lowered in magnitude compared to the blank sample, but did not have an opposing behavior as Figs. 2 and 4; however, this different behavior may be attributed to its not being calcined. Hence, calcination may be a cause of the opposite absorbance behavior.

4. Conclusions

The successful fabrication of a dip-coated TiO_2 photocatalyst onto glass Raschig rings remains to be a challenge, as the appropriate binder and coating conditions would have to be improved in ensuring good dispersion of catalyst and achieving a filmlike coating. The changing absorbance behavior of the calcined photocatalyst is suggested to be caused by the calcination process, brought about by the decomposition of organics present in the uncalcined catalyst.

Acknowledgments

The authors thank Adolph Bravo Jr., Ervin Cezar and Darlene Que for the fabrication of TiO_2-coated Raschig rings.

The authors would also like to express their gratitude to Dr. Rizalinda de Leon for the use of the FTIR in the UP Diliman Chemical Engineering Laboratory and David Gonzales and Jay R Adolacion for their help in performing the FTIR analyses.

References

[1] K. Nagaveni, G. Sivalingam, M.S. Hegde and G. Madras, Appl. Catal. B. Environ. Lett. **48** (2004) 83-93.

[2] A. Fujishima, X. Zhang and D.A. Tryk, Surf. Sci. Rep. **63** (2008) 515-582.

[3] H. de Lasa, B. Serrano and M. Salaices, 2005. Photocatlytic Reaction Engineering. USA: SpringerLink.

[4] Kounvong, K., Dalida, M.P., Bajamundi, C.E., Hinode, H. (2011). *Removal of Color in Water Solution using TiO2 Photocatalyst.* Unpublished manuscript.

Effect of Foil Thickness on Mechanical Property of Pure Copper Foil

Asuka Yokoyama[*1], Tomoyuki Fujii[*1], Keiichiro Tohgo[*1],
Yasuhiro Noda[*2] and Yoshinobu Shimamura[*1]

[*1]Shizuoka University Department of Mechanical Engineering
3-5-1 Johoku Naka-ku, Hamamatsu, 432-8561.Japan
[*2]Rengo Co., Ltd
e-mail: ayokoyama@mechmat.eng.shizuoka.ac.jp

1. Introduction

Pure copper foil is widely applied to the electrical wiring in printed circuits, negative-electrode material in lithium-ion cell and so on. It is important to evaluate the mechanical properties of the copper foil because they are used in severe mechanical and electrical loading. Many investigations of the mechanical properties of copper foil were reported. It was noted that deformation and fracture behavior of the metallic foils were different from those of bulk materials because of their unique micro-structure. It is important to clarify the mechanical properties of the metallic foil to evaluate their integrity in service.

In this study, tensile tests of pure copper foils were conducted to evaluate fracture behavior and clarify the effect of foil thickness on the deformation and fracture behavior.

2. Experimental procedure

2.1 Material

Cold rolling copper foils (99.96% copper) whose thickness is 5μm, 10μm, 50μm and 2mm. The specimen shape was rectangle for copper foil and dog-bone shape for copper sheet. The tensile detection was rolling direction. The grain diameter of all specimens was set to about 20μm by heat treatment.

2.2 Tensile testing

Tensile tests were conducted at room temperature and crosshead speed 0.5mm/min. The elongation was measured by a non-contact extensometer. After the tensile tests, fracture surface was observed by scanning electron microscope in order to investigate the fracture morphology.

3. Results and Discussion

3.1 Stress-strain curves

Figure 1 shows nominal stress – strain curves at each thickness. All specimens showed large elastic deformation. The tensile strength and strain at tensile strength decrease with decreasing foil thickness. Figure 2 shows the tensile strength as a function of foil thickness. The foil thickness is normalized by grain diameter. The tensile strength was constant when the thickness was thicker than grain diameter. However, tensile strength goes down rapidly when the thickness was thinner than grain diameter.

3.2 Fracture morphology

Figures 3(a) and (b) shows the fracture morphology of thickness of 10μm and 50μm, respectively. The intergranular fracture occurred in thickness of 10μm. In the case of 5 μm, the same fracture morphology was also observed. On the other hand, the chisel point fracture occurred in thickness of 50μm. This result agrees the fracture morphology of common metallic materials.

The effect of foil thickness on tensile strength is explained as follows: when the thickness is thicker than foil thickness, the local necking occurs, and then chisel point fracture occurs. The large plastic deformation occurs and the tensile strength is high. On the other hand, when the foil thickness is thinner than grain diameter, the intergranular fracture occurred. Therefore, the plastic deformation during tension is terminated and the tensile strength is low.

4. Conclusion

The tensile tests for four kinds of thickness of copper foil were conducted in order to evaluate their mechanical properties. The

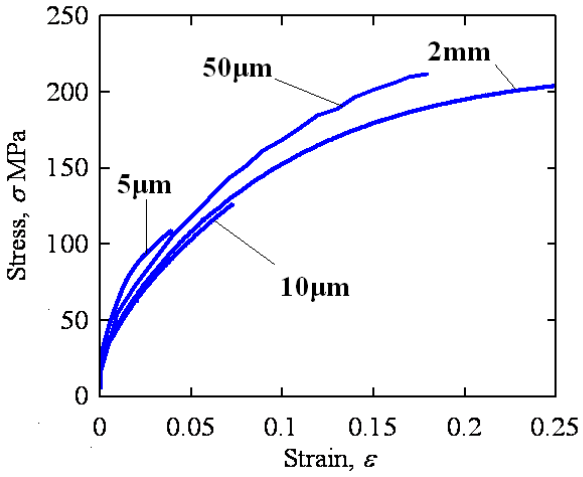

Fig. 1 Stress – strain curves of copper foil.

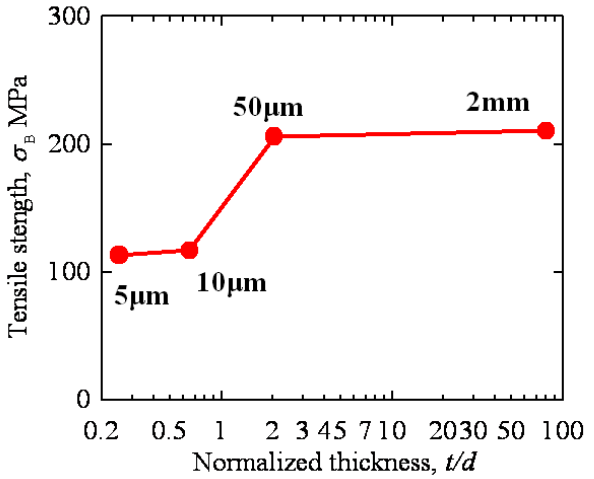

Fig. 2 Tensile strength as a function of normalized thickness

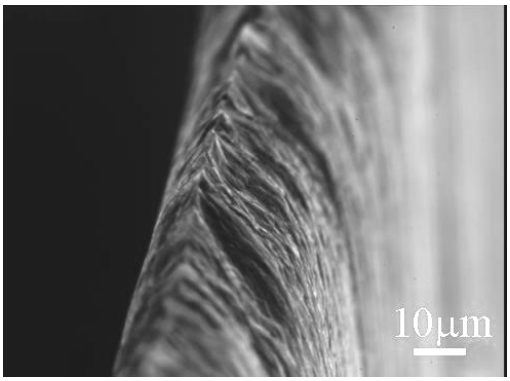

(a) Foil thickness of 50μm.

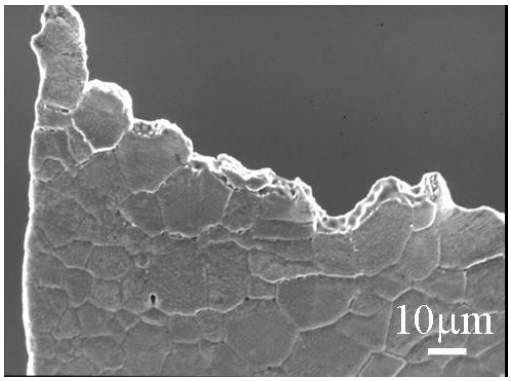

(b) Foil thickness of 10μm.

Fig. 2. Fracture morphology of copper foil.

conclusions obtained in this investigation are summarized as follows.

1. The tensile strength and strain at tensile strength decreased when the foil thickness was thinner than grain diameter.
2. The chisel point fracture occurred when the foil thickness was thicker than grain diameter. On the other hand, the intergranular fracture occurred when the foil thickness was thinner than grain diameter.

Reference

1. H. Harada, Y. Z.Ssun, Y. Sakamoto, Y. Marumo, L. Ruan. Slide-bending formation of thin metal sheet by using an industrial robot, Transactions of the Japan Society of Mechanical Engineers, C, Vol.73, No.734(2007), pp.2834-2840.
2. T. Sano, K. Toyama, H. Kimachi, T. Iai, K. Tanaka and Y. Akiniwa. Evaluation of fracture strength by crack initiation and propagation on grain boundary in polycrystals, Transactions of the Japan Society of Mechanical Engineers, No.55 (2006), pp.123-124.
3. B. Weiss, V. Groger, G. Khatibi, A. Kotas, P. Zimprich, R.Stickler, B. Zagar. Characterization of mechanical and thermal properties of thin cu foils and wires, Sensors and actuators, A, No.99(2002), pp.172-182.

Fatigue Property of Jute MonoFilament

Kazunori UEMATSU*, Yoshinobu SHIMAMURA
Hideaki KATOGI, Keiichiro TOHGO and Tomoyuki FUJII

Department of Mechanical Engineering, Shizuoka University
3-5-1 Johoku, Naka-ku, Hamamatsu, Shizuoka 432-8561, Japan
*e-mail: kuematsu@mechmat.eng.shizuoka.ac.jp

1. Introduction

In recent years, with the growing interest in environmental issue, composite materials from natural sources have been developed. However, superior strength and fatigue properties are necessary to alternate traditional load-bearing structures. Therefore, fatigue strength of natural fiber reinforced composites should be investigated. In order to elucidate the fatigue property of the composites, it is necessary to clarify fatigue property of natural fibers. In this study the fatigue property of jute mono filament was investigated.

2. Structure of Natural Fiber

Figure 1 shows a schematic of typical natural elementary fiber. Open hole, called lumen, exists in the center of an elementary fiber. Microfibril (MF) is a bundle of cellulose, which is bonded by hydrogen bonding, surrounds around cell walls. MF has an angle to the axial direction, which determines the axial stiffness. MFs are adhered by hemicelluloses and lignin. Monofilament consists of elementary fibers that are adhered by pectin.

3. Specimen

Alkaline treatment was performed for washing jute yarns. Jute filaments were extracted from the washed yarns. The diameter of a Monofilament was measured from two perpendicular directions along the length. The cross sectional area of a fractured portion was estimated by elliptical approximation using the above data.

4. Tensile Test of Jute Filament

Qausi-static tensile tests were conducted at room temperature. The cross head speed was 1mm/min and the gauge length was 10mm. Table 1 shows the mechanical properties.

Table1. Mechanical property

Tensile strength [MPa]	Young modulus [GPa]
448	16

5. Fatigue Test of Jute Filament

Fatigue testing was conducted at room temperature. Loading frequency was 10Hz and the gauge length was 10mm. The stress ratio is 0.1 and the maximum stress was 60 to 120% of the tensile strength.

Figure 2 shows S-N diagram. The error bar at 10^0 cycles is the standard deviation of the tensile strength.

Fatigue strength at 10^6 cycles was about 50% of the tensile strength. Therefore, fatigue property of jute Monofilaments is considered to be superior. Figure 3 shows the fracture portion after fatigue testing. Splitting among elementary fibers and pull out of secondary wall in an elementary fiber were found.

6. Conclusions

(1) Jute Monofilament has superior fatigue property.
(2) Splitting between elementary fibers and pull out of secondary wall were found after fatigue failure.

Reference

(1) M. M. Meyers, P.-Y. Chen, A.Y.-M. Lin andY. Seki, *Progress in Materials Science* 53 (2008) pp.1-206

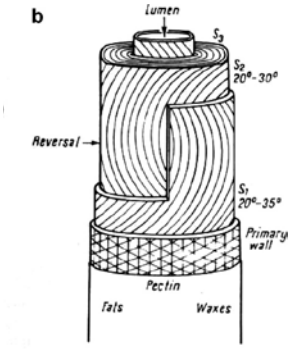

Fig.1 Structure of natural-fiber[1]

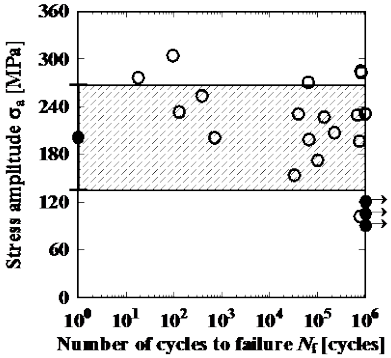

Fig.2 S-N diagram of jute filament

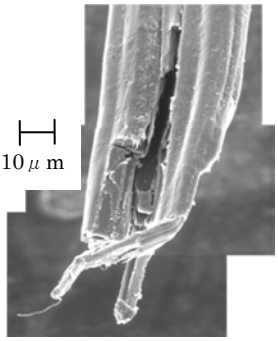

Fig.3 Jute filament after fatigue

Synthesis of Furfural from Pineapple Bagasse

Emmanuel Belostrino*, Billy Joe Uy, Mark Louis Lagura and Terence Tumolva

Department of Chemical Engineering, University of the Philippines
Diliman 1101 Quezon City, Philippines
TELEFAX: +632-929-6640
*e-mail: epbelostrino@upd.edu.ph

1. Introduction

Because of the continuous decline in reserves and increase of prices of fossil fuels, significant amounts of research are done globally to produce chemicals from alternative renewable sources. Agricultural waste materials prove to be a viable option as a potential source of valuable organic chemicals such as sugars, ethanol and basic components of polymer resins.

Furfural is produced by the hydrolysis of xylose-rich materials. It is an essential chemical because of its use as a selective solvent for the separation of saturated and unsaturated compounds in fuels. Moreover, it is also used to derive other valuable chemicals such as furfuryl alcohol, which is the monomer for furan resins, which is a biothermoset.

Previous researches have been conducted to determine the viability of producing furfural through acid hydrolysis of different agricultural residues such as corn cobs, rice hulls, sugar bagasse, and fruit shells [1].

Fig. 1. Pineapple bagasse.

In the Philippines, pineapple is considered as one of the country's major agricultural products, with an annual production of approximately two million metric tons. The xylose-rich pineapple bagasse produced from juice manufacturing plants is a potential viable source of raw material in the synthesis of furfural. This research is the first step in the study of the feasibility of locally manufacturing furfural and furfuryl alcohol in the Philippines.

2. Acid Hydrolysis of Pineapple Bagasse

The pineapple bagasse was crushed and 0.1 g of the sample was placed inside a 10 mL reaction tube. 3.5 mL of 2 M H_2SO_4 was then added in the tube and was tightly covered. Hydrolysis of the sample was carried out in a 180 ºC oil bath. For each run, varying reaction times were observed (3 min, 6 min, 9 min, 12 min, 15 min).

After the desired reaction time, the reaction tube was cooled in a water bath and was filtered. A few drops of hot water was added to wash the precipitate. 20 mL of 2,4-dinitro phenyl hydrazine solution was added to the furfural-containing filtrate. A brown precipitate (furfural 2,4-dinitro phenyl hydrazine) formed and was weighed [2]. The furfural yield was then calculated. Two trials were performed for each run.

3. Results and Discussion

Figure 2 shows the furfural yield of pineapple bagasse as a function of hydrolysis time. The results show that the yield increases linearly with hydrolysis time (with R^2 = 0.9779). For a hydrolysis period of 15 minutes, the maximum yield obtainable is about 11.53%.

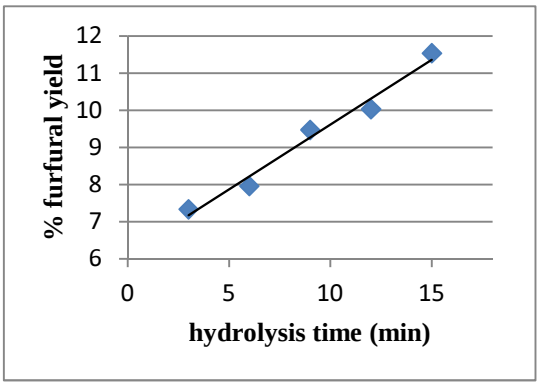

Fig. 2. Furfural yield of pineapple bagasse a function of hydrolysis time.

The effects of acid concentration and reaction temperature on the furfural yield are also to be investigated in the next phase of the project- this is to determine the most ideal conditions that would lead to maximum furfural yield.

4. Conclusion

Pineapple bagasse is a viable raw material for the production of furfural. Increasing the hydrolysis time increases the furfural yield. The yield can be further maximized by varying the acid concentration and reaction temperature to optimize the hydrolysis process.

References

[1] H. Mansilla, J. Baeza, S. Urzua, G. Maturana, J. Villaseñor and N. Duran, Acid-Catalyzed Hydrolysis of Rice Hull: Evaluation of Furfural Production, Bioresource Technology, **66** (1998) 189-193.

[2] A. Demirbas, Furfural Production from Fruit Shells by Acid-Catalyzed Hydrolysis, Energy Sources, Part A, **28** (2006) 157-165.

Fatigue Strengh of a Paper-based Friction Material under Shear-Compressive Loading

Naoya URATA, Jun SHIBATA, Tomoyuki FUJII, Keiichiro TOHGO
and Yoshinobu SHIMAMURA

Dept. of Mechanical Engineering, Shizuoka University
3-5-1 Johoku, Naka-ku, Hamamatu, Shizuoka, 432-8561, Japan
e-mail: nurata@mechmat.eng.shizuoka.ac.jp

1. Introduction

Paper-based friction materials are used for clutch disc of an automatic transmission. Paper-based friction materials are subject to cyclic shear-compressive loading under elevated temperature in oily environment. It is important to clarify their fatigue properties under the cyclic shear-compressive loading to evaluate their remaining life in services.

This paper deals with the fatigue strength under the cyclic shear-compressive loading to evaluate their fatigue properties. The influence of ratio between shear and compressive stress on the fatigue strength was evaluated.

2. Experimental Procedure

2.1 Material

A paper-based friction material is composed of aramid fibers and phenolic resin. The material includes the aramid fiber of 70wt% and phenolic resin of 30wt%, and the porosity was 72.2%. The thickness was 0.5±0.02mm or 1.5±0.02mm. The materials were prepared by bonding two sheets of aluminum alloy on both surfaces.

2.2 Shear-compressive test

The specimens were subjected to the compressive load at an inclined angle of as shown in Fig. 1. The stress Σ, resolved shear stress σ, and compressive stress τ, are defined in Fig. 1. The cyclic frequency was 10Hz and the sinusoidal load with the loading ratio of R=0.1 was applied. When the specimens are not broken at 10^6 cycles, the fatigue test is terminated and this condition is regarded as the fatigue strength for 10^6 cycles.

2.3 Cyclic compressive loading behavior

Compressive deformation tests were carried out in order to discuss the fatigue strength. The tests were carried out under the pure compressive cyclic load with the stress ratio of 0.1 and applied load rate of 0.1kN/min. The maximum load increased stepwise by 1.0kN up to 10kN. The compressive load was repeated five times at the same load level, and hysteresis loops of the fifth cycle were examined.

3. Results and Disscusion

3.1 Fatigue strength

Figure 2 shows the relationship between the stress range $\Delta\Sigma$ and the number of cycles N. The fatigue strength decreases with increasing the number of cycles. With increasing inclined angle θ, the compressive stress becomes dominant and then the fatigue strength increases.

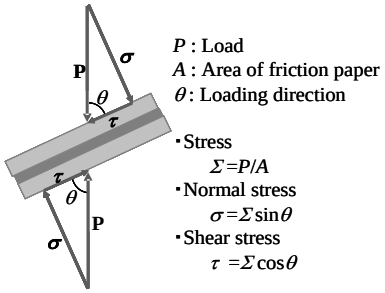

Fig.1Loading condition.

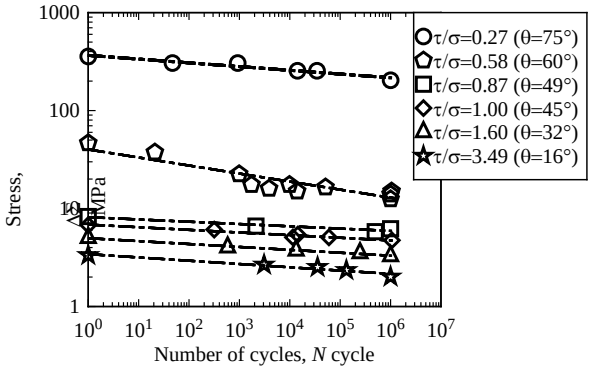

Fig.2 S-N curves of the paper-based friction material under shear-compressive loading.

3.2 Compressive Deformation Property

The hysteresis loops of cyclic deformation test under pure compressive load are shown in Fig. 3. With increasing stress level, the hysteresis loop shifts to the high strain direction and its gradient becomes steep.

For each hysteresis loop, the unloading elastic modulus is defined as a slope of the unloading relation from the maximum stress and the strain range $\Delta\varepsilon$ are defined as the range between strain at maximum stress and at minimum stress. Figure 4 shows the maximum strain ε_0, strain range $\Delta\varepsilon$, elastic modulus E as functions of the maximum compressive stress. the maximum strain and Young's modulus increased with increasing maximum compressive stress, while the strain range remained as constant low value. These results are explained as follows: the paper-based friction material is a porous material with porosity of about 70%. The porosity decreases with increasing compressive stress, and then the friction materials become dense and the elastic modulus becomes high. Therefore, the gradient of the hysteresis loops becomes steep and the strain range does not increase as compared with an increase in the stress range. The reason why the fatigue strength of the paper-based friction material is remarkably high under the compressive-dominant stress condition is attributed to their characteristics of the compressive cyclic deformation as mentioned above.

4.Conclusion

The static fracture and fatigue tests of the paper-based friction material were conducted under the various shear-compressive loading conditions, and the influence of loading conditions on the static fracture strength, fatigue strength and fracture surface morphology were discussed. Furthermore, the cyclic compressive deformation behavior was examined to explain the fatigue strength of the paper-based friction material under compressive-dominant stress condition. The conclusions obtained in this investigation are summarized as follows.

1. The fatigue strength decreases with increasing the number of cycles. The fatigue strength is higher when the compressive stress is more dominant.
2. In the pure compressive cyclic deformation tests, when the stress range increased the gradient of the hysteresis loops becomes steep and the strain range does not increase. Therefore, it is considered that the fatigue strength is remarkably high when the compressive stress is dominant.

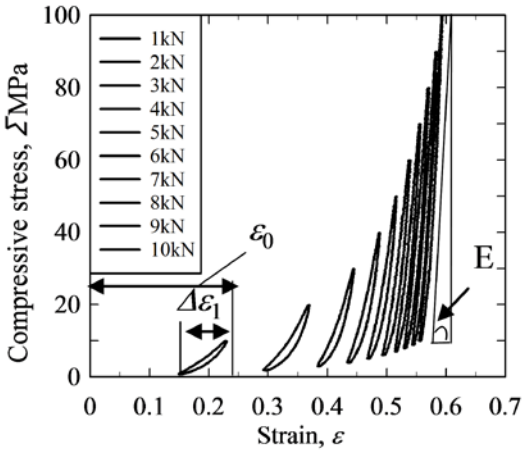

Fig.3 Stress-strain hysteresis loop of compressive cyclic deformation.

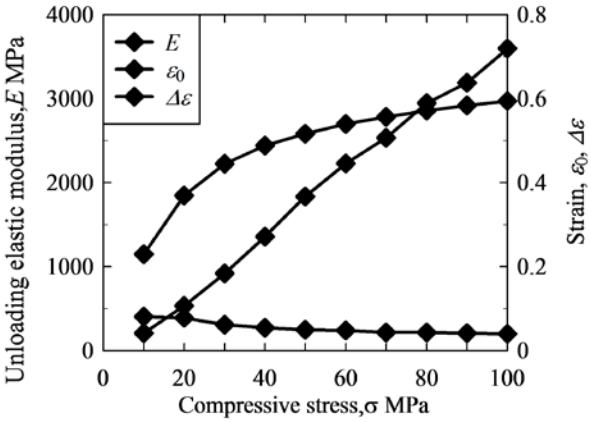

Fig.4 Young's modulus, maximum strain and strain range as functions of compressive stress.

Synthesis of Furfural from Coconut Shells

Billy Joe Uy*, Emmanuel Belostrino, Mark Louis Lagura,
Rodel Guerrero, and Terence Tumolva

Department of Chemical Engineering, College of Engineering, University of the Philippines,
Diliman, Quezon City 1101, Philippines
TEL&FAX: +06-981-8500
*e-mail: byuy@upd.edu.ph

1. Introduction

Coconut in the Philippines is popularly known as the "Tree of Life" because of the wide array of products and by-products that can be derived from the tree. Some of these products are coconut meat, oil, juice, husk, shell, shell charcoal, leaves, husk, pith, inflorescence, trunk and roots. The coconut shell is a treated as a byproduct in the production of nut, copra and coconut oil. It is currently used as a shell charcoal for domestic and commercial fuel. It is said that there are more than 300 million coconut trees in the Philippines that produces an annual average of 15 billion nuts. [3]

Fig. 1. Crushed coconut shells.

Furfural is produced from the pentosan fraction of the lignocellulosic materials that are natural and abundant natural resource. Pentosan from nonfood residues of food crops and wood wastes are first converted into pentoses from monosaccharides by acid hydrolysis and further dehydration of these pentoses will yield furfural. Furfural is currently used as a direct solvent in petroleum refining and also in the production of phenolic resins. Furfural is also an important intermediate in the synthesis of valuable solvents such as furfuryl alcohol (a monomer of biosynthetic furan resin), furfurylic alcohol and tetrahydrofuran (THF).

Chemicals that are derived from non-food agricultural residues like furfural are essential in obtaining a self-sustaining industry. With the rapid consumption and continuous decline of the supply for fossil fuels, finding alternative renewable resources is vital in any industry.

2. Acid Hydrolysis Experiment for Coconut Shells

The crushed air-dried sample of the shell was placed inside a 5 mL test tube and was tightly sealed. 3.5 mL of 2M sulfuric acid was then added before heating in an oil bath at 180°C. The hydrolysis time (3, 6, 9, 12 and 15 min) were varied to observe its effect to the furfural yield. The test tube was then promptly cooled in a water bath and the product was filtered and then washed with hot water.

Furfural was precipitated from the solution by adding 2,4-dinitro phenyl hydrazine solution. The brown precipitate (furfural 2,4-dinitro phenyl hydrazine) was then filtered and weighed to compute for the furfural yield.

3. Results and Discussion

A plot of the furfural yield with varying hydrolysis time is shown in Figure 2. A trend line with an R^2=0.6104 is obtained which indicate the low level linearity of the points. This can be due to the presence of errors and the degree of violence of the reactions. It can be seen however that the yield increases as the hydrolysis time increases. The peak yield was 12.4% from the 15 min hydrolysis time.

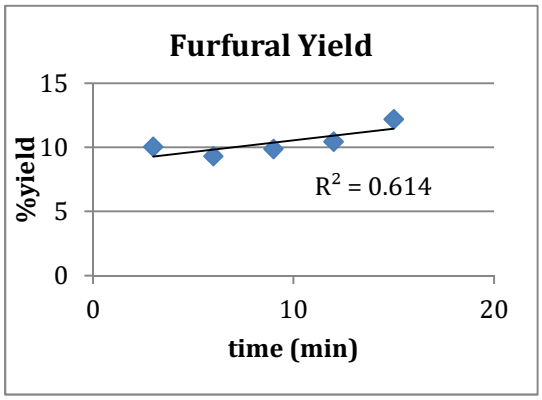

Fig. 2. Furfural Yield from Coconut shells with varying hydrolysis time

Linearity of the data points can be improved by having a better experiment setup and by performing more trials per run. Variables that may affect the yield of furfural such as the temperature and acid concentration should be investigated to further enhance the yield of furfural.

4. Conclusion

Coconut shells prove to be a suitable raw material for the production of furfural that has yielded a maximum value of 12.4%. An increase in the hydrolysis time also showed an increase in the yield of furfural. Optimization of the process and manipulation of other variables could further increase the yield of furfural synthesized from coconut shells.

Reference

[1] A. Demirbas, Furfural Production from Fruit Shells by Acid-Catalyzed Hydrolysis, Energy Sources, Part A, 28 (2006) 157-165.
[2] M. Kazemi, Furfural Production from pisthachio green hulls as agricultural residues, October 2009.
[3] Philippine Coconut Authority, Department of Agriculture (www.pca.da.gov.ph)

Evaluation of Mechanical Properties of PSZ-Ti Biocompatible Composite Fabricated by MIM Method

Kazufumi NAKAZAWA[1*], Tomoyuki FUJI[1], Keiichiro TOHGO[1], Masaki ISHIKURA[2] and Yoshinobu SHIMAMURA[1]

[1] Dept. of Mechanical Engineering, Shizuoka University
3-5-1 Johoku, Naka-ku, Hamamatu, Shizuoka, 432-8561, Japan
[2]Nippon Kinzoku .Co.Ltd
[*]e-mail: knakazawa@mechmat.eng.shizuoka.ac.jp

1. Introduction

Partially stabilized zirconia(PSZ) and pure titanium(Ti) are expected as implant materials due to biocompatibility. However, homogeneous materials fabricated by PSZ or Ti are insufficient to satisfy characteristics required for medical use.

This paper deals with fabrication of composites consisting of Ti and PSZ to derive their good characteristics of both materials. The composites were fabricated by metal injection modeling. Indentation and three-point bending tests were conducted to evaluate fracture toughness. The reaction products were identified by X-ray diffraction analysis.

2. Experimental procedure

2.1 Fabrication method

PSZ powders with the grain size of 0.35 μm and pure Ti powders with the grain size of 24 μm were used as raw materials. These powders were mixed in various volume ratios covering from 100% PSZ to 100% Ti at prescribed interval. The composites were fabricated through the processes of forming, debinding and sintering.

2.2 Fracture toughness test

The fracture toughness was measured by indentation test and three-point bending test. The cracks were introduced from the corner of the indent, and the fracture toughness was calculated by IF method when the Ti volume fraction was less than 90%. On the other hand, the fracture toughness was measured by three-point bending test because no crack was introduced by using the indentation tests when the Ti volume fraction was more than 90%.

3. Experimental results

3.1 Fracture toughness

Figure 1 shows the relationship between the fracture toughness and the Ti volume fraction. The fracture toughness decreased with increasing of Ti volume fraction when the Ti volume fraction was less than 90%. On the other hand, the fracture toughness increased with increasing of Ti volume fraction when the Ti content was more than 90%.

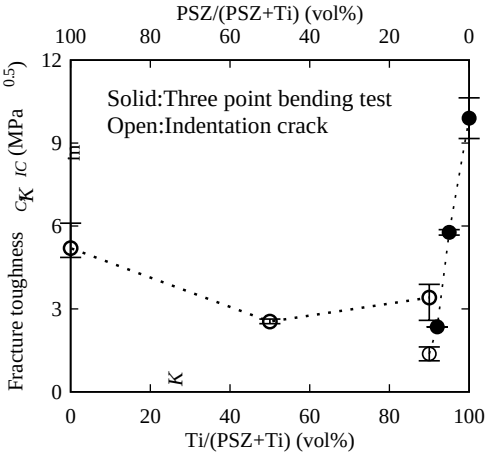

Fig. 1 Fracture toughness as a function of Ti volume fraction.

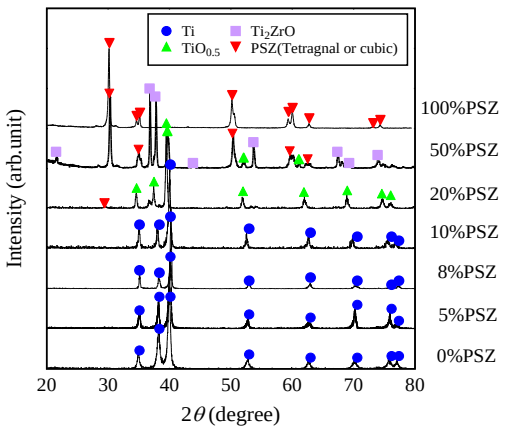

Fig. 2 XRD patterns of the sintered materials.

3.2 Phase constitution of composites

Figure 2 shows the XRD patterns after sintering. When the Ti volume fraction was less than 90%, the oxide of titanium and other reaction products were formed after sintering. The composites might be brittle because of these reaction products. However, pure titanium remained after sintering when the Ti volume fraction was more than 90%, and the composites characterized by relatively high ductility.

Evaluating Carbon Storage Potential in Furfural Synthesis

Rodel D. Guerrero* and Terence P. Tumolva

Department of Chemical Engineering, University of the Philippines,
Diliman 1101 Quezon City, Philippines
TELEFAX: +6329296640
*e-mail: rodeldayagguerrero@gmail.com

1. Introduction

Mitigating the contribution of fossil fuel emissions to global warming has been and is still a great environmental concern. Large quantities of carbon dioxide, CO_2, which is believed to be one of the key greenhouse gases that promote climate change, is being released into the atmosphere from the use of fossil fuel in power generation and other industries. Thus, a large number of researches have been already conducted for finding out ways to reduce CO_2 emissions.

Among the current trend in line with the aim of reducing carbon dioxide in the atmosphere is the production of bio-based products, particularly polymers. These materials are proven to beneficial given their ability to 'fix' the carbon content of the material, making them carbon neutral. Bio-based polymers or bioplastics can either be thermoplastic or thermosetting in nature, but in terms of tonnage, the bulk of plastics produced are thermoplastics.

Thermoplastics are known to have low to non-existent polymer chain interactions thus making it readily vulnerable to reactions. These plastics can be only used for short-term applications, which is why thermosets are preferred for long-life applications. However, the production of non-biodegradable bio-based thermosets for applications that require persistent materials has been given little attention so far, although there is a demand for large amounts of these materials [3].

Polyfurfuryl alcohol (PFA) is a biosynthetic thermoset derived from vegetable byproducts. Compared to other common resins, this highly stable polymer offers a very significant improvement in the carbon storage potential of green composites when used as a matrix. PFA is polymerized from furfuryl alcohol derived from furfural, which is manufactured from agricultural residues such as sugar cane, bagasse, oat hulls, corn cobs and rice hulls.

Since carbon storage potential in terms of CO_2 fixation is a key environmental parameter evaluated in this study, certain Life Cycle Analysis (LCA) principles are applied on the material to serve as a guide and tool for the evaluation of carbon storage potential. However, analyses of this kind are mainly concerned on the overall CO_2 emission and not on the bio-based carbon content of the material [1]. So in this paper, a quantification of the extent of carbon fixation from the synthesis of furfural derived from pineapple bagasse will be investigated. As such, measurements of the carbon dioxide released during the furfural's synthesis due to fossil fuel consumption for energy supply will be calculated.

2. Carbon Balance

As a biosynthetic thermoset, it is strongly believed that PFA has the capacity to store carbon from biomass produced by the utilization of atmospheric CO_2 by plants during photosynthesis. However, as with any industrial process, the manufacture of this material entails the use of energy, which translates to CO_2 emission that could easily offset the effectiveness of furan to sequester CO_2 as stored bio-based carbon [1]. Therefore, it is also important to identify the different pertinent flow streams of carbon and the energy consumption throughout the entire production process of the monomer of PFA which is furfural. This can be done by calculating the net bio-based carbon content or *E(NB)* of the material as well as the

energy generated during the process which has its equivalent amount of CO_2 emission mainly due to the consumption of fossil fuels to generate the energy.

3. Results and Discussion

The hydrolysis time for the synthesis of furfural from the pineapple bagasse lasted for about 15 minutes.

Figure 1. Furfural synthesis set up.

Table 1. Carbon balance for furfural production.

Items	Value	Unit
CO_2 production	0.0050277	g
Fossil-based carbon equivalent, F	0.001371	g
MW of furfuryl alcohol, $C_5H_4O_2$	96.08	g/mol
Wt. furfural produced	0.01198	g
Weight C in furfural	0.007481	g
Bio-based carbon equivalent, B	0.007481	g
Total carbon content equivalent, E(T) = F + B	0.008852	g
Bio-based carbon content equivalent, E(B) = B/(F + B)	0.8451	g/g
Net bio-based carbon content equivalent, E(NB) = B – F	0.00611	g

4. Conclusion

Carbon storage exhibited by the synthesis of furfural was evaluated using the information obtained from carbon balance. The potential of carbon sequestration exhibited by the furfural synthesis for the raw material- pineapple bagasse- proved to be an environment-friendly process for which the carbon fixation of the polymerization of such monomer would be of great interest in future researches.

Reference

[1] T. Tumolva, M. Kubouchi, S. Aoki, and T. Sakai (2011). “Evaluating the Carbon Storage Potential of Furan Resin-Based Green Composites”. *18th International Conference on Composite Materials.*

[2] Demirbas, A. (2006). “Furfural Production from Fruit Shells by Acid-Catalyzed Hydrolysis.”

[3] Steinbuchel, A. (2005). Non-biodegradable biopolymers from renewable resources: perspectives and impacts. *Science Direct*

[4] "IPCC Special Report Carbon Dioxide Capture and Storage Summary for Policymakers". *Intergovernmental Panel on Climate Change*. Retrieved 2011-10-05.

Mechanical property of unidirectional MWNT sheet/epoxy composites

M. Sakai[1*], Y. Shimamura[1], N. Morisawa[1], K. Tohgo[1] and T. Fujii[1]

[1]Department of Mechanical Engineering, Shizuoka University,
3-5-1 Johoku, Naka-ku, Hamamatsu, Shizuoka 432-8561, Japan
[*]e-mail: msakai@mechmat.eng.shizuoka.ac.jp

1. Introduction

Carbon nanotubes (CNT) have high specific strength, stiffness, and low density, and are anticipated to exceed the mechanical properties of carbon fibers, which is mainly used for composite materials in aerospace industry. Therefore, CNTs attract attention in various fields. In the field of composite, CNTs are expected as high performance reinforcement materials, and widely investigated for the last decade.

In this study, multi-walled carbon nanotube (MWNT) sheets developed by Inoue et al [1] were used as preform for making composites. The mechanical properties were investigated by tensile tests and SEM observation.

2. Materials and Specimen

MWNT arrays were grown on a substrate by chemical vapor deposition (CVD method). MWNT sheets are fabricated from the MWNT array. Thickness and specific density of MWNT sheets were about 15 μm and 0.4, respectively. Bisphenol-A type epoxy resin with high-temperature cure was used for matrix.

The hand lay-up method was used to fabricate composites. Unidirectional MWNT sheets were laid on a Teflon sheet and then resin was impregnated. After curing, composite plate was cut into rectangular specimens. Then, a specimen as glued onto a paper mount to fix the specimen. Fiber volume contents (V_f) of composites were calculated by fiber mass contents that had been measured by thermo gravimetrical analysis.

The cross-head speed was 1mm/min at room temperature. Displacement was measured by using a noncontact extensometer.

3. Results and Discussion

Figure 1 shows typical stress-strain curves of resin, MWNT sheet and composite specimens with different V_f. Table 1 shows the average Young's modulus and tensile strength. Figure 2 shows a SEM image of a fracture surface of a composite specimen with V_f=13.7%.

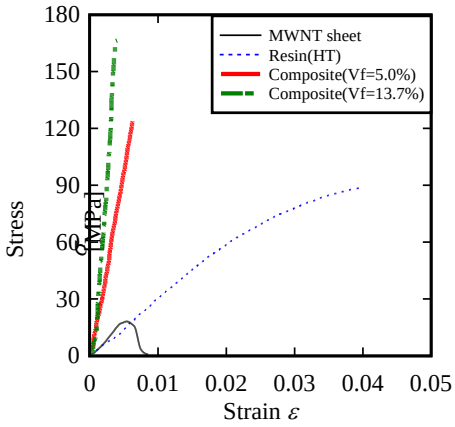

Fig.1 Stress-strain curves.

Table.1 Mechanical properties.

	resin	MWNT sheet	Composite (Vf=5.0%)	Composite (Vf=13.7%)
Young's modulus[GPa]	2.5	3.9	15.4	31.1
Tensile strength[MPa]	81.2	17.7	117.0	136.8

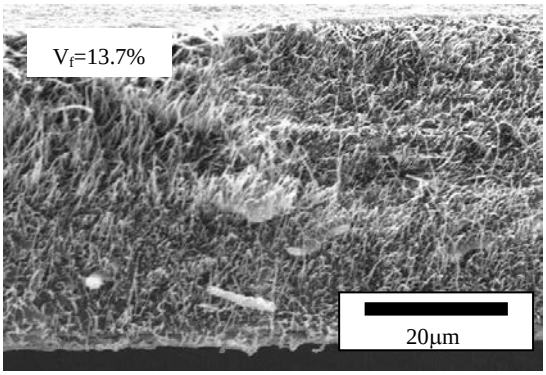

Fig.2 Fracture surface of composite (V_f =13.7%).

The enhancement of Young's modulus and tensile strength were confirmed. In particular, Young's modulus of composites with V_f=13.7% was about 12 times as much as that of resin. From the fractograph, wettability of epoxy into MWNTs and well alignment of CNTs in composite were confirmed.

4. Conclusions

Using MWNT sheets as preform enables us to enhance mechanical properties remarkably. The further mechanical properties are expected by increasing V_f.

References

[1] Y. Inoue, K. Kakihata, Y. Hirono, T. Horie, A. Ishida, and H. Mimura, *APPLIED PHYSICS LETTERS*, 92 (2008), 213113

Evaluating the Carbon Storage Potential of NFRP Using Water Hyacinth Fiber Reinforcement

Joseph Ortenero* and Terence Tumolva

Department of Chemical Engineering, University of the Philippines
Diliman 1101 Quezon City, Philippines
TELEFAX: +6329296640
*e-mail: josh_42786@yahoo.com

1. Introduction

The use of natural fiber as reinforcement has significant advantages, among others are in increasing mechanical properties, reducing cost, biodegradability and especially the renewability and sustainability of the reinforcement. Currently, there is a great abundance of research on natural fiber-reinforced plastic (NFRP). However, most of these studies are focused on mechanical property and thermal property evaluations and only a small percentage is devoted to data collection on environmental advantages in the area of carbon sequestration with the use of renewable bio-based material. In this study, it is attempted to develop a systematic approach to evaluating the carbon storage potential of water hyacinth reinforced composite. Figure 1 shows a sample of water hyacinth plant.

Fig. 1. Water hyacinth (*Eichhornia crassipes*) is considered an invasive species, which invades fresh water habitats and is listed along with some of the worst weeds.

Water hyacinth was introduced as an ornamental crop species in many countries more than a century ago. Soon, it was realized to be an invasive species due to their adaptability to a wide type of fresh water ecosystems and interference with human activities. However, it was recently realized that they could be sustainably managed in their natural ecosystem and used as reinforcement in NFRP's.

2. Carbon Balance

The effectiveness of water hyacinth fiber (WHF) in sequestering carbon was measured in terms of equivalent carbon content. The method adopted for evaluating carbon storage potential was through the calculation of the net bio-based carbon content of the material. Net bio-based carbon content assessment is a more direct representation since it expresses stored carbon in terms of carbon weight fraction within the material.

3. Result and Discussion

Water hyacinth is low in lignin content (10%) and contains high amounts of cellulose (20%) and hemicelluloses (33%). The carbon content of water hyacinth was estimated based on the average fraction of cellulose in the fiber and the weight percent of carbon in the cellulose. The calculation on net bio-based carbon content was shown in Table 1. The average cellulose content of water hyacinth is around 25%. Carbon is in the order of 52% of the cellulose fiber. Therefore, carbon safely sequestered by a water hyacinth

plant is 0.013 kg per kilogram of NFRP composite considering 10% loading of WHF in the NFRP composite. For the estimation of carbon content in orthophthalic unsaturated polyester (ortho-UP), certain assumptions were imposed to simplify calculations based on a published C-NMR study on the crosslinking of UP with styrene. The amount of carbon emission in the form of carbon dioxide for the production of the polymer matrix was based on a previously reported list of gross energy requirements for different intermediates and plastics.

Table 1. Carbon balance for the fabrication of water hyacinth-reinforced NFRP

Items	Value	Unit
Wt. percent water hyacinth fibers in NFRP	10.0	%
Wt. water hyacinth fibers/kg NFRP	0.100	kg
Wt. fraction cellulose in water hyacinth fiber	0.250	kg/kg
Wt. percent C in cellulose	52.0	%
Wt. C from abaca fibers	0.013	kg
Wt.UP resin matrix/kg NFRP	0.900	kg
Wt.C from ortho-UP	0.604	kg
Fossil based carbon equivalent	1.19	kg
Bio-based content in NFRP	10.0	%
Bio-based carbon equivalent	0.013	kg
Total carbon content equivalent	1.203	kg
Biobased carbon content equivalent	0.011	kg/kg
Net biobased carbon content equivalent	-1.177	kg

4. Conclusion

Evaluation of carbon storage potential of thermoset-based NFRP composite is vital for assessing the environmental impact of a material. The carbon storage potential of NFRP can be easily increased by increasing WHF content.

References

[1] S Bolenz, H Omran, K Gierschner (1990) "Treatment of water hyacinth tissue to obtain useful products" Biowastes 33:263-274

[2] T. Tumolva, M. Kubouchi, S. Aoki, T. Sakai, "Evaluating the Carbon Storage Potential of Furan Resin-Based Green Composite", 18th International Conference on Composite Materials

Tensile Property of Carbon Nanotube Spun Yarn Reinforced Composite

Kahori Oshima[1], Yoshinobu Shimamura[1], Keiichiro Tohgo[1], Tomoyuki Fujii[1], Mikihisa Ishihara[1], Yoku Inoue[2] and Junichi Muramatsu[2]

[1] Department of Mechanical Engineering, Shizuoka University, 3-5-1 Johoku Naka-ku, Hamamatsu, 432-8011, Japan

[2] Department of Electrical and Electronic Engineering, Shizuoka University

1. Introduction

Carbon nanotubes (CNTs) are expected to exceed the mechanical properties of conventional carbon fibers, but growing continuous CNTs have limitation so far. Consequently, it is difficult to apply CNTs to structural components. In order to solve this matter, techniques of spinning have been investigated. However, the basic mechanical properties of CNT spun yarn have not been clarified.

In this study, tensile tests of CNT spun yarn were conducted and stress-strain curves were obtained to investigate the mechanical behavior of CNT spun yarn. In addition, CNT composite was fabricated by using the pultrusion technique, and tensile tests of CNT composite were carried out.

2. Materials

Multi walled carbon nanotubes (MWNTs) used in this study were grown on a quartz glass plate with chemical vapor deposition (CM-CVD method), using C_2H_2 and $FeCl_2$ as a material and a catalyst, respectively [1]. It was possible to draw out MWNTs from array by Van der Waals' force. The MWNT length was around 1.2mm and the diameter was 50nm. The spun yarn diameter was about 45μm. Twist angle α is defined as an angle of MWNT of outermost layer to the longitudinal axis of a spun yarn.

Generally, it is known that properties of a spun yarn depend on the twist angle. In this study, a spun yarn that the twist angle α=25~30° was used. Room- temperature curing epoxy was used for fabrication of MWNT composite.

3. MWNT Composite

3.1 Fabrication of MWNT Composite

MWNT composites were fabricated by using the pultrusion technique. Figure 1 shows a schematic of pultrusion process of MWNT composites. The advantages of this method are able to remove extra resin on a MWNT bundle and also to form a cylindrical shape at the same time. In this study, 7 spun yarns were used because it was the effective number of spun yarn for maximizing a volume fraction; a hexagonal close-packed structure is achieved. Loading tensile force to MWNT composites while curing is effective for getting specimens straight and for restraining the expansion of yarn.

A die was made in a plastic board for the pultrusion, and an end of a MWNT bundle was laced through the die. The MWNT bundle was dipped into resin and then plutluded. After that, a weight was attached to an end of the bundle as dead load while curing. The diameter of MWNT composite was about 120μm.

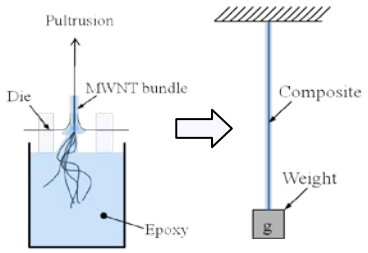

Fig.1 Pultrusion process of MWNT composite

3.2 Tensile Test

A MWNT composite specimen was placed on a U-shaped paper mount. The both ends of the specimen were glued with adhesive. The gauge length was 15mm. The paper mount was cut in a half after the specimen was fixed to a testing machine, and then tensile tests were conducted. The tests were carried out at room temperature and cross head speed was 1mm/min. Strain was measured by using a non-contact

extensometer.

Figure 2 shows a stress-strain curve of MWNT composites and individual materials. Maximum Young's modulus of MWNT composite was 56.2GPa and maximum tensile strength was 432MPa. These values were about 10 and 7 times as high as those of resin, respectively. Tensile behavior of MWNT composite was more linear than that of MWNT spun yarn. It implies that resin was well impregnated into MWNT spun yarns. This means that tensile properties of MWNT composites are dominated by the tensile properties of MWNTs.

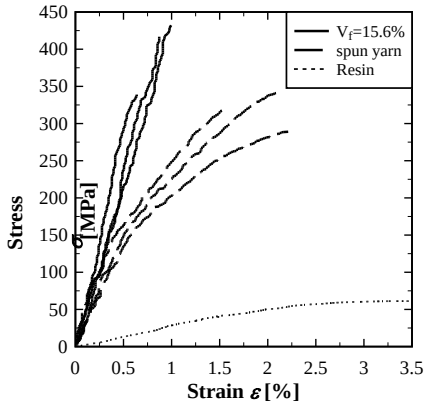

Fig.2 Stress-strain curve of MWNT composite and individual materials

4. Conclusions

- The pultrusion technique of spun yarn is an effective method for increasing a volume fraction in fabrication of MWNT composite.
- Tensile properties of MWNT composites are dominated by the tensile properties of MWNTs if resin is well impregnated into MWNT spun yarns.

Reference

[1] Y. Inoue, K. Kakihata, Y. Hirono, T. Horie, A. Ishida, and H. Mimura, *APPLIED PHYSICS LETTERS*, 92 (2008), 213113